


# Dual-mode imaging and therapeutic effects of drug-loaded phase-transition nanoparticles combined with near-infrared laser and low-intensity ultrasound on ovarian cancer

Shuning Chen<sup>a,b\*</sup> , Yujiao Liu<sup>a\*</sup>, Shenyin Zhu<sup>c</sup>, Chunyan Chen<sup>a</sup>, Wan Xie<sup>a</sup>, Linlin Xiao<sup>a</sup>, Yi Zhu<sup>a</sup>, Lan Hao<sup>b</sup>, Zhigang Wang<sup>b</sup>, Jiangchuan Sun<sup>a</sup> and Shufang Chang<sup>a</sup>

<sup>a</sup>Department of Obstetrics and Gynecology, The Second Affiliated Hospital of Chongqing Medical University, Chongqing, PR China; <sup>b</sup>Institute of Ultrasound Imaging, Second Affiliated Hospital of Chongqing Medical University, Chongqing, PR China; <sup>c</sup>Department of Pharmacy, The First Affiliated Hospital of Chongqing Medical University, Chongqing, PR China

## ABSTRACT

Chemotherapy and photo-sonodynamic therapy (PSDT) can be combined through drug delivery nano-platforms to enhance the anti-tumor efficacy, however, which is limited by hypoxia in tumor, thereby causing chemotherapy resistance. Perfluoropentane (PFP) has the ability to carry oxygen and to enhance ultrasound or photoacoustic imaging after vaporization. Herein, we constructed a kind of nanoparticles (PTX/ICG and oxygen loaded PLGA nanoparticles (PIO\_NPs)), which had PFP core carrying oxygen and PLGA shell loaded indocyanine green (ICG) and paclitaxel (PTX). PIO\_NPs harbored good optical stability and the ability to transit phase. Moreover, it could rapidly release PTX and generate ROS under the mediation by near-infrared laser and low-intensity ultrasound. The PIO\_NPs enhanced contrast of the ultrasound and PA imaging. In particular, PIO\_NPs may be used to monitor and guide treatment for the accumulation of PIO\_NPs at tumor site can be observed by PA imaging. Compared with PTX or other nanoparticles, PIO\_NPs combined with laser and ultrasound (L.U) significantly induced apoptosis of SKOV3 cells and inhibited SKOV3 tumor growth. Therefore, PIO\_NPs are of great potential in cancer imaging and therapy.

## ARTICLE HISTORY

Received 11 June 2018  
Revised 26 July 2018  
Accepted 29 July 2018

## KEYWORDS

Paclitaxel; indocyanine green; phase-shift nanoparticles; hypoxia; dual-mode imagin

## 1. Introduction

Ovarian cancer is one of the most prevalent gynecologic malignancies with high incidence and mortality rates (Torre et al., 2015; Siegel et al., 2017). The standard treatment for ovarian cancer encompasses maximal cytoreductive surgical debulking followed by administration of paclitaxel (PTX)-platinum based chemotherapy. However, lack of early diagnosis and chemotherapy resistance tend to contribute to the high recurrence rate and poor prognosis of patients (Tew et al., 2014; Kampan et al., 2015; Cortez et al., 2018).


Combination therapy, combining two or more therapies together, has a great potential for improving therapeutic efficiency and overcoming drug resistance. Previous studies have explored the combination of photodynamic therapy (PDT) or sonodynamical therapy (SDT) and chemotherapy (Zheng et al., 2013; Huang et al., 2014; Su et al., 2015). Photo-sonodynamic therapy (PSDT) is a novel modality for cancer treatment, aimed at enhancing anticancer effects by the combination of PDT and SDT. By activating con-generous sensitizers with light and sound, PDST produced more obvious anti-cancer effects than any monotherapy, and further

decreased the dosage of sensitizer and the energy of ultrasound or light which can further reduce the side effects (Wang et al., 2009; Tserkovsky et al., 2012; Li, et al., 2013, Wang et al., 2015; Liu et al., 2016a; Tang et al., 2017). Therefore, PSDT was used in our study as a more effective treatment. In spite of the complicated mechanism of PDST, the production of reactive oxygen species (ROS) is one of the key factors. Intracellular ROS production threatens the integrity of various biomolecules (Tomankova et al., 2009), leading to cellular damage and dysfunction (Kim et al., 2013; Di Meo et al., 2016). However, the effect of combination of PSDT and chemotherapy is rarely explored.

PTX is one of the main drugs for ovarian cancer chemotherapy (Kampan et al., 2015). Due to its high insolubility in water and severe anaphylactic reactions, its clinical applications are limited (Raisch et al., 2011). Indocyanine green (ICG) is a proven con-generous sensitizer of PSDT that responds to near-infrared light and ultrasound (Nomikou et al., 2012; Tang et al., 2017). Due to its low toxicity, ICG has been approved by the FDA for clinical application. However, the fast body clearance (plasmatic half-time of 2–4 min) and instability in water solution are considered as the main

**CONTACT** Shufang Chan  [shfch2005@163.com](mailto:shfch2005@163.com); Jiangchuan Sun  [sunjiangchuan@126.com](mailto:sunjiangchuan@126.com)  Department of Obstetrics and Gynecology, The Second Affiliated Hospital of Chongqing Medical University, 74 Linjian Road, Yuzhong District, Chongqing 400010, PR China

\*These authors contributed equally to this work.

 Supplemental data for this article can be accessed [here](#).

© 2018 The Author(s). Published by Informa UK Limited, trading as Taylor & Francis Group.  
This is an Open Access article distributed under the terms of the Creative Commons Attribution License (<http://creativecommons.org/licenses/by/4.0/>), which permits unrestricted use, distribution, and reproduction in any medium, provided the original work is properly cited.

drawbacks of using ICG (Polom et al., 2011; Porcu et al., 2016). Liquid perfluorocarbon (PFC) compounds are good oxygen carriers (Riess, 2006) and can be vaporized using acoustic or optical droplet vaporization methods (Krafft, 2001; Sun et al., 2014). To improve the therapeutic effect, we consider the combination of PTX, ICG, and PFC through the drug delivery platform. And poly (lactic-co-glycolic acid) (PLGA) is a good choice for a drug delivery vehicle because of its biocompatibility and safety. Moreover, several studies have demonstrated that dyes-loaded or drug-loaded PLGA nanoparticles can induce PDT/SDT or enhance cytotoxicity (McEwan et al., 2014; Heo et al., 2015; Pakulska et al., 2016; Abou-ElNaga et al., 2017). Herein, our ideal drug delivery platform is based on PLGA, which has the following advantages: (1) high drug loading efficiency; (2) PTX-based chemotherapy combined with ICG-based PDT; (3) oxygen carried PFC improve hypoxia of tumor (McEwan et al., 2015; McEwan et al., 2016); (4) controlled drug release.

Due to the moderate fluorescence quantum yield of ICG (Porcu et al., 2016) and its absorption of NIR range, it has been suggested as a contrast agent in photoacoustic (PA) imaging. As a noninvasive imaging technique that converts optical signals into sound signals, PA imaging has great potential for disease diagnostic and therapeutic monitoring (Valluru et al., 2016). Various photosensitizer nano-composites have been used for PA imaging (Cho et al., 2010; Liu et al., 2016b; Zhang et al., 2016; Lemaster & Jokerst, 2017). Among them, ICG-based nanoparticles can be used as PA contrast agents due to their intense and stable signal (Chen et al., 2016; Gao et al., 2016; Deng et al., 2017). After being vaporized *via* optical irradiation and acoustic pressure, PFC can change its phase and subsequently generate gas (Krafft, 2001). And based its phase-shift ability, some studies synthesized PFC-loaded particles to enhance ultrasound images (Lin et al., 2017) and PA images (Wilson et al., 2012). Furthermore, a photosensitizer and PFC loaded particle can enhance dual mode imaging which combines PA and ultrasound imaging (Hannah et al., 2014; Chen et al., 2016; Lin, et al., 2017).

In this study, we constructed a nanoparticle with an oxygen-containing perfluoropentane (PFP) liquid core and PTX/ICG loaded PLGA shell. On the one hand, it can remarkably promote anti-tumor effects and effectively reduce drug resistance. Exposure to NIR and ultrasound contributed to controlled release of PTX and generation of ROS, localized treatment, and minimized side effects. On the other hand, based on the optical properties of ICG and the phase-shift capability of PFP, the nanoparticle can be a promising tool for dual mode imaging. This nanoparticle harbored a potential to integrate imaging diagnostics and anti-tumor therapy and to realize medical imaging-guided visual diagnosis and treatment.

## 2. Materials and methods

### 2.1. Materials

PTX was purchased from Nantong Feiyu Biotechnology (Jiangsu, PR China). ICG was purchased from Aladdin

(Shanghai, PR China). PLGA (lactide: glycolide = 50:50, molecular weight = 12,000 Da) was obtained from the Shandong Key Laboratory of Medical Polymer Materials (Shandong, PR China). Perfluoro-*n*-pentane (PFP) was obtained from Fluka (St Louis, MO). Polyvinyl alcohol (PVA, 87–90%) was purchased from Sigma-Aldrich Co. (St Louis, MO). Singlet oxygen sensor green (SOSG) was obtained from Thermo Fisher Scientific (Waltham, MA). 3-(4,5-dimethylthiazol-2-yl)-2,5-diphenyltetrazoliumbromide (MTT), 2-(4-amidinophenyl)-6-indolecarbamidine dihydrochloride (DAPI) and 2',7'-dichlorofluorescein diacetate (DCFH-DA) were all purchased from Beyotime Biotechnology (Shanghai, PR China). All other reagents were commercial products of analytical grade.

### 2.2. Methods

#### 2.2.1. Preparation of particles

PTX/ICG and oxygen loaded PLGA nanoparticles (PIO\_NPs) were prepared using a modified double emulsion (water/oil/water) evaporation process according to previous studies (Tang et al., 2017). Saturated ICG aqueous solution and 200  $\mu$ L PFP bubbled with oxygen gas were mixed using an ultrasonic probe (Sonics & Materials, Inc., Fairfield, CT) for 1 min. The mixture was bubbled with oxygen again. Next, the mixture was added to methylene chloride (2 mL) dissolving PLGA (50 mg) and PTX (3 mg) and emulsified using ultrasonic probe at 120 W for 3 min. Then, the above-described emulsified solution was poured into PVA solution (4% w/v) and sonicated again to produce second emulsion. The final emulsion was stirred for 4 h to sufficiently extract methylene chloride. Subsequently, the solution was centrifuged at 12,000 rpm for 5 min at 4 °C (Biofuge Stratos Centrifuge; Thermo Fisher Scientific, Germany), followed by washing by deionized water of the precipitate. The process of centrifugation was repeated three times until the supernatant was clarified. The washed precipitate was re-suspended in 5 mL oxygen-enriched PBS and stored at 4 °C for further use. The IO\_NPs (ICG and oxygen loaded PLGA nanoparticles) were prepared without PTX similarly. The O\_NPs (only oxygen loaded nanoparticles) were prepared without ICG and PTX. PI\_NPs (PTX and ICG loaded PLGA nanoparticles) were prepared omitting the oxygen saturation processes. All procedures were carried out under low temperature and dim light.

#### 2.2.2. Characterization of the NPs

The NPs size (diameter, nm), polydispersity index and surface charge (zeta potential, mV) were measured by dynamic light scattering using a Malvern Zetasizer Nano ZS unit (Malvern Instruments, Malvern, UK) at room temperature. In addition, these indicators of PIO\_NPs were determined after laser irradiation (808 nm, 1.5W/cm<sup>2</sup> for 2 min). The morphology of PIO\_NPs with or without laser irradiation was obtained by microscopy (Eclipse Ti, Nikon Corporation, Tokyo, Japan). The morphology of PIO\_NPs was also detected by scanning electron microscope (SEM, FEI Inspect F50, FEI Company, USA), and transmission electron microscope (TEM, FEI Tecnai G2 F20, FEI Company, USA).

The LE and EE of PTX were detected by HPLC analysis. A C18-column was used with a mobile phase composed of acetonitrile and water (70: 30, v/v) and flow rate of 1.0 mL/min. The LE and EE of ICG were determined in triplicate by an ultraviolet-visible (UV-Vis) spectrophotometer (260-Bio, Thermo Fisher Scientific). The absorbance of non-entrapped ICG in the supernatant was measured at 780 nm. The mass of entrapped ICG was equal to mass of total ICG minus the mass of non-entrapped. The LE and EE were calculated according to the following formulas: LE (%) = (weight of loaded drug/total weight of NPs) × 100, EE (%) = (weight of loaded drug/weight of initially added drug) × 100.

The absorption spectra and the fluorescence spectra of free ICG and PIO\_NPs were detected in PBS and 10% fetal bovine serum by similar procedure in previous studies (Zheng et al., 2011; Ma et al., 2017). The absorption spectra were determined by UV-Vis spectrophotometer (wavelength from 650 to 850 nm). The fluorescence spectra were obtained by fluorescence spectrometer (Cray Eclipse, Agilent Technologies) with excitation at 740 nm, meanwhile, the emission spectra were recorded from 760 to 860 nm. Furthermore, to monitor the degradation of ICG in different samples, the absorbance (at 780 nm) and the fluorescence intensity (at maximal emission wavelength) of samples were recorded every 3 d for 15 d.

*In vitro* PTX release profile of PIO\_NPs was also determined by HPLC. The 1 mL PIO\_NPs was placed into vial containing 50 mL of phosphate buffered saline (PBS, pH 7.4). The vials, containing equal PIO\_NPs, were shaken continuously for 48 h at 120 rpm and 37 °C. Then samples were ultra-centrifuged and collected at the indicated time points (0, 2, 4, 8, 12, 24, 36, and 48 h). We also measured PTX release behavior after NIR irradiation (808 nm, 1.5W/cm<sup>2</sup> for 2 min) and ultrasound exposure (1.0 MHz, 1W/cm<sup>2</sup>, 1 min). The PTX content was measured using the same HPLC method as above.

The SOSG reagent was highly selective for <sup>1</sup>O<sub>2</sub>. In the presence of singlet oxygen, it emitted green fluorescence (excitation/emission maxima ~504/525 nm). The SOSG and free ICG, O\_NPs, PI\_NPs, or PIO-NPs were mixed into MilliQ water to obtain working concentrations of 5 μM SOSG and 5 μg/mL ICG in final solution. Next, the solution was irradiated with 1.5W/cm<sup>2</sup> 808 nm for 2 min and exposed to 1.0 W/cm<sup>2</sup> low-intensity for 1 min (The role of laser and ultrasound [L.U]). Finally, singlet oxygen, before and after explosion to L.U, was determined by measuring the fluorescence intensity using a fluorescence microplate reader (Varioskan Flash, Thermo Fisher Scientific).

### 2.2.3. Therapeutic effect in vitro

The human ovarian cancer SKOV3 cell line was kindly offered by Professor Ronald X. Xu at University of Science and Technology of China (Hefei, Anhui). Cells were maintained in RPMI 1640 culture medium containing 10% fetal bovine serum, 1% penicillin, and 1% streptomycin at 37 °C under 5% CO<sub>2</sub>. Cells in the exponential phase of growth were used for all experiments.

SKOV3 cells (1 × 10<sup>6</sup> cells/well) were seeded into a six-well plate and incubated overnight. Then, the medium was

replaced by the free medium containing ICG (1.73 μg/mL) or PIO\_NPs (containing ICG 1.73 μg/mL, PTX 3.64 μg/mL). After 4 h incubation, the cells were washed thrice with PBS and fixed with 4% paraformaldehyde for 15 min. The nuclear dye DAPI was used as a positive control to stain nuclei in the experiment. Finally, the cells were observed under confocal laser scanning microscope (CLSM, Leica TCS SP8, Heidelberg, Germany). Similarly, SKOV3 cells were treated and subjected to flow cytometry.

To determine the role of apoptosis in response to different NPs combined with L.U, we assessed the apoptosis of cells after treatment using Annexin V-fluorescein isothiocyanate (FITC)/PI double staining, followed by analysis of flow cytometer. Briefly, the SKOV3 cells were seed into six-well plate in 1 mL of medium and cultured for 24 h. Next, the medium was removed and replaced by 250 μL culture media containing equivalent concentrations of free PTX, IO\_NPs, PI\_NPs, and PIO\_NPs (final ICG concentration 3.46 μg/mL, PTX 7.28 μg/mL). After 4 h incubation, sterile PBS was used to wash cells thrice and each well was added with new complete medium. Then the treated cells were irradiated with 1.5W/cm<sup>2</sup> 808 nm for 2 min and exposed to 1.0 W/cm<sup>2</sup> low-intensity for 1 min (The role of L.U). Cells were collected after 24 h of treatment and re-suspended with staining solution containing V-FITC and PI. All samples were incubated at room temperature in dark for 15 min and analyzed by flow cytometer.

Intracellular ROS productions were determined by using 2',7'-dichlorofluorescein diacetate (DCFH-DA) assay. Briefly, SKOV3 cells were seed in six-well plate (1 × 10<sup>6</sup> cells/well) and incubated overnight. Next, cells were incubated with PTX, IO\_NPs, PI\_NPs, or PIO\_NPs for 4 h. The cells were washed three times by using PBS and incubated by DCFH-DA (10 μM) in dark for 30 min. Unloaded DCFH-DA was discarded and replaced by medium. The test samples were exposed to L.U, followed by observation by fluorescence microscope. After interacted with intracellular ROS, DCFH changed to DCF with green fluorescence. In addition, fluorescence microplate reader was employed to determine the fluorescence intensity at excitation of 485 nm and emission of 528 nm.

### 2.2.4. Imaging in vivo

Some similar tumor-bearing nude mice were anesthetized with 1% sodium pentobarbital. Then, B-mode and PA-mode imaging were performed using VEVO LASR PA imaging system (VIVO 2100, FUJIFILM Visual Sonic, Inc., Bothell, WA). The mice were divided into 3 groups (n = 3), which were injected with PBS, free ICG or PIO\_NPs through tail vein. Images were obtained at 2, 4, 6, 12, 14, 48, and 72 h, respectively. In addition, in order to explore the changes in the imaging after laser irradiation, the tumors were subjected to NIR irradiation (1.5W/cm<sup>2</sup>, 5 min) at the best imaging time (6 h), followed by analysis of the echo intensity (EI) in B-Mode using DFY (invented by the Institution of Ultrasound Imaging of Chongqing Medical University) and the PA average value using the VEVO LASR PA imaging system (VIVO 2100, FUJIFILM Visual Sonic, Inc., Bothell, WA).

### 2.2.5. Therapeutic effect in vivo

Female BLAB/c athymic nude mice, 6–7 weeks of age and 18–20 g of weight, were purchased from Chinese Academy of Medical Science (Beijing, China). SKOV3 cells in logarithmic growth phase were trypsinized, washed twice, and suspended in sterilized PBS. The 200  $\mu$ L cell suspension ( $5 \times 10^7$  cells/mL) was injected into flank of each mouse. The experiments were all conducted in compliance with Practice Guidelines for Laboratory Animals of China.

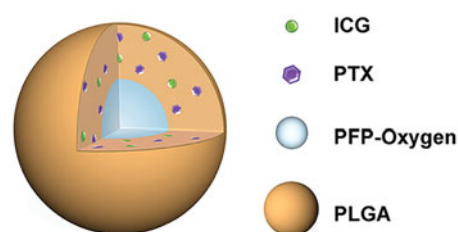
Ten days after tumor growth, the tumor volume reached about 500 mm<sup>3</sup>. The following formula was used to estimate tumor volume: length  $\times$  width<sup>2</sup>  $\times$  0.5. Then these mice were randomly divided into five groups (eight mice per group) and injected different drugs of 300  $\mu$ L through tail vein. Specifically, the treatment groups were as follows: (1) control (saline); (2) PTX (only PTX); (3) PI\_NPs + L.U (applying PI\_NPs combined L.U); (4) IO\_NPs + L.U (applying IO\_NPs combined L.U); (5) PIO\_NPs + L.U (applying PIO\_NPs combined L.U). The PTX dose (5 mg/kg) was kept consistent in these above treatment groups. For groups (3), (4), and (5), 808 nm laser (1.5W/cm<sup>2</sup>, 5 min) and low-intensity ultrasound (1W/cm<sup>2</sup>, 1 min) were applied 6 h after injection. Treatment was performed every 5 d for a total of four times. Body weight and tumor volume were recorded every three days throughout the treatment circle.

Twenty-four hours after the last treatment, three mice were sacrificed randomly in each group. Their tumor tissues and organs (heart, liver, spleen, lung, and kidney) were harvested and fixed in 4% paraformaldehyde for paraffin clines. Hematoxylin and eosin (H&E) staining was used for histopathological analysis. Terminal-deoxynucleotidyl Transferase Mediated Nick End Labeling (TUNEL) assay was performed to detect apoptosis in tumor cells, and apoptotic index (AI) was used to show the results. The tumor tissue sections were stained with antibodies against CD34 (polyclonal, 1:1000, Abcam, Cambridge, UK) and VEGF (polyclonal, 1:200, Affinity, Sterling, VA) to detect the microvascular density. The result of VEGF was expressed using IOD integrated optical density (IOD). And the microvessel density (MVD) was determined by calculating all CD34 positive vessels. The pictures were obtained by a digital camera and analyzed by software Image Pro Plus version 6.0 (Media Cybernetics, Inc., Rockville, MD, USA).

Western blot was used to detect the expression of HIF-1 $\alpha$  and MDR-1 in tumor tissues. Additionally, the remaining five mice in each group were observed until natural death, and the survival time of each mouse was recorded.

### 2.3. Statistical analysis

Graphpad Prism version 6.0 (La Jolla, CA) software was used to analyze the experimental results. The data were expressed as mean  $\pm$  standard deviation (SD) and analyzed by one-way analysis of variance (ANOVA). The differences among the means in *in vivo* experiments were evaluated by the Tukey Kramer multiple comparison test. Survival rates of different treatment groups were illustrated by the Kaplan–Meier



**Scheme 1.** Schematics illustration of the PIO\_NPs. PLGA: poly (DL-lactide-co-glycolic acid); PFP-oxygen: perfluoro-n-pentane carried oxygen; PTX: paclitaxel; ICG: indocyanine green; PIO\_NPs: paclitaxel, indocyanine green and oxygen loaded nanoparticles.

curves and compared by the Log-rank Test. A *P* value of less than .05 was considered as statistically significant.

## 3. Results and discussion

### 3.1. Characterization of the NPs

The schematic structure of PIO\_NPs was shown in Scheme 1. The PIO\_NPs contained a liquid oxygen-saturated PFP core and the PLGA shell loaded ICG and PTX. And the optical microscopy image, size distribution, and zeta potential of PIO\_NPs were acquired (Figure 1(a), and red line in Figure 1(b,d)). The phase change was then performed by 808 nm laser irradiation, and the nanoparticles were measured again (Figure 1(c), and blue line in Figure 1(b,d)). After PIO\_NPs triggered by laser irradiation to phase transition, its size was significantly increased and the zeta potential was slightly increased. SEM image and TEM image of PIO\_NPs are shown in Figure 1(e,f). The results showed that PIO\_NPs were generally spherical in shape with good monodispersity. As shown in Table S1, the average diameter of PIO\_NPs was  $186.4 \pm 1.9$  nm; and the average zeta potential was  $-19.43 \pm 0.55$  mV. The drug encapsulation efficiency (EE) and drug loading efficiency (LE) of PTX or ICG were also shown. For PIO\_NPs, the EE and LE of PTX were  $64.29 \pm 2.76$  and  $3.64 \pm 0.16\%$ , the EE and LE of ICG were  $57.27 \pm 0.77$  and  $1.73 \pm 0.15\%$ . As an ideal phase-changeable drug-loaded nanoparticle, PIO\_NPs not only encapsulate PTX and ICG, but also can be triggered to phase transition by laser irradiation. These properties of other nanoparticles including IO\_NPs and PI\_NPs were compared with PIO\_NPs (Table S1), and the LE and EE of ICG or PTX were lower than those of PIO\_NPs.

The optical properties of PIO\_NPs were determined. The absorption spectrum of free ICG and PIO\_NPs was shown in Figure 1(i), while the fluorescence spectra were shown in Figure 1(k). Although the ICG entrapped into PLGA (PIO\_NPs) exhibited a near-infrared absorption with absorbance peak at 790 nm, the absorption peak was hypochromic-shifted 10 nm approximately. On the other hand, the emission peak of PIO\_NPs was changed almost 6 nm whose peak was red-shifted from 788 to 804 nm. We also investigated the optical stability of free ICG and PIO\_NPs, measured the absorption and emission spectra separately every 3 d, which revealed that free ICG was degraded faster than PIO\_NPs. After 15-d observation, PIO\_NPs decreased the intensity of absorption by about 25%, while free ICG was decreased nearly 80% (Figure 1(j)). In addition, compared with free ICG, PIO\_NPs have better

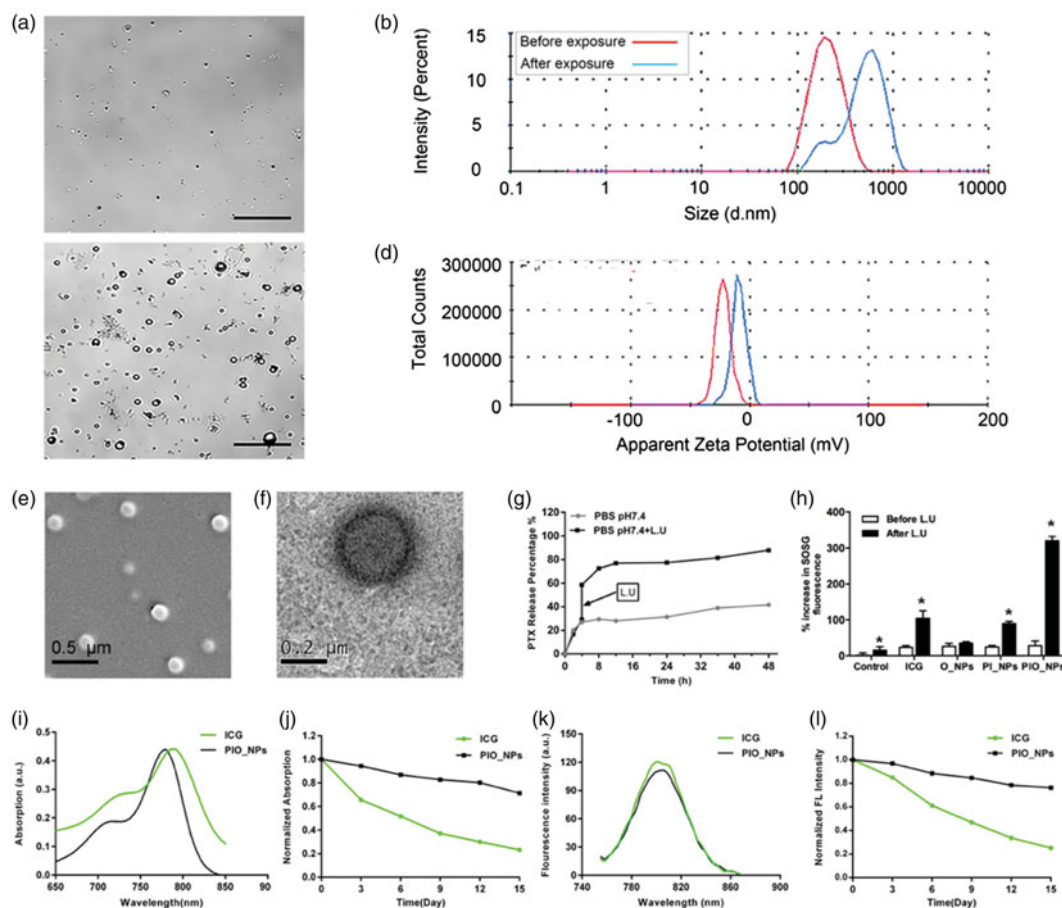


**Figure 1.** Optical microscopy images before (a) and after (b) laser irradiation, scale bar of microscopy images are 10  $\mu\text{m}$ . Size distributions (c) and zeta potential (d) were detected before (red line in pictures) and after (blue line in pictures) laser irradiation. SEM (e) images of PIO\_NPs, the scale bar is 0.5  $\mu\text{m}$ . TEM (f) images of PIO\_NPs, the scale bar is 0.2  $\mu\text{m}$ . The release of PTX with or without L.U exposure (g), percentage increase of SOSG fluorescence intensities for control, free ICG, O\_NPs, and PIO\_NPs in MilliQ water with or without L.U exposure (h). The role of laser and ultrasound (L.U). Error bars represented  $\pm$  the standard error where  $n = 3$ . \* $p < .05$  versus each group without L.U. Absorbance spectra of free ICG and PIO\_NPs (i), absorbance stability test of free ICG and PIO\_NPs (j), fluorescence spectra of free ICG and PIO\_NPs (k), and fluorescence stability test of free ICG and PIO\_NPs (l).

absorption stability in 10% fetal bovine serum. (Figure S2). The fluorescence intensity of PIO\_NPs was decreased by about 20%, but free ICG was decreased by nearly 80% (Figure 1(l)). After the ICG loaded into the nanoparticles, its absorption and fluorescence stability were significantly improved, which was favorable for the long-term storage.

To further investigate the potential of PIO\_NPs for chemotherapy and PDT, we measured the release of PTX and the production of singlet oxygen after L.U exposure. At 37  $^{\circ}\text{C}$  and pH 7.4, only 41.65% PTX released after 48 h. However, the release of PTX was increased from 29.04 to 58.58% with L.U exposure at 4 h, finally reaching 86.65% at 48 h (Figure 1(g), Figure S1), which indicated that PTX release was faster when mediated by L.U. SOSG was used for detecting production of singlet oxygen based on its fluorescence changing. A plot of percentage increased in SOSG fluorescence before and after L.U treatment for PBS, free ICG, O\_NPs, PI\_NPs, and PIO\_NPs was shown in Figure 1(h). After exposure, the SOSG fluorescence intensity revealed a significant increase for PIO\_NPs (319.76%) when compared with free ICG (104.1%), O\_NPs (35.21%), or PI\_NPs (89.99%). It suggested that the production of singlet oxygen was not only due to the excitation of the ICG, but also depended on the supply from PFP carried oxygen.

### 3.2. Therapeutic effect in vitro

The cell uptake behavior of free ICG or PIO\_NPs was observed by confocal laser scanning microscope. As shown in Figure 2(a), cells incubated with PIO\_NPs exhibited stronger intracellular green fluorescence signal. Due to instability of ICG, cells incubated with free ICG exhibited weak intracellular green fluorescence signal. In addition, it is possible to remove part of the ICG in the medium by washing three times with PBS. For the PIO\_NPs group, a large number of PIO\_NPs had been up-taken by the cells. And in bright image, there were many visible particles in cytoplasm. Further quantitative analysis by flow cytometry (Figure S3) revealed a significant increase of fluorescence intensity in PIO\_NPs group. The mean fluorescence intensity of the PIO\_NPs group was about 15 times that of the ICG group. These results demonstrated that PIO\_NPs can be uptake into SKOV3 cells and also keep its fluorescence characteristic.

The cell viability was detected by MTT assay after different treatment for 24 h. Compared with PTX, PIO\_NPs containing the same concentration of PTX reduced cell viability to a great extent (Figure S4(a)). This may be due to that PIO\_NPs were effectively uptake by cells while PTX was slowly released. After exposure to L.U, the cell viability was further reduced in PIO\_NPs group. Combined with L.U, PIO\_NPs

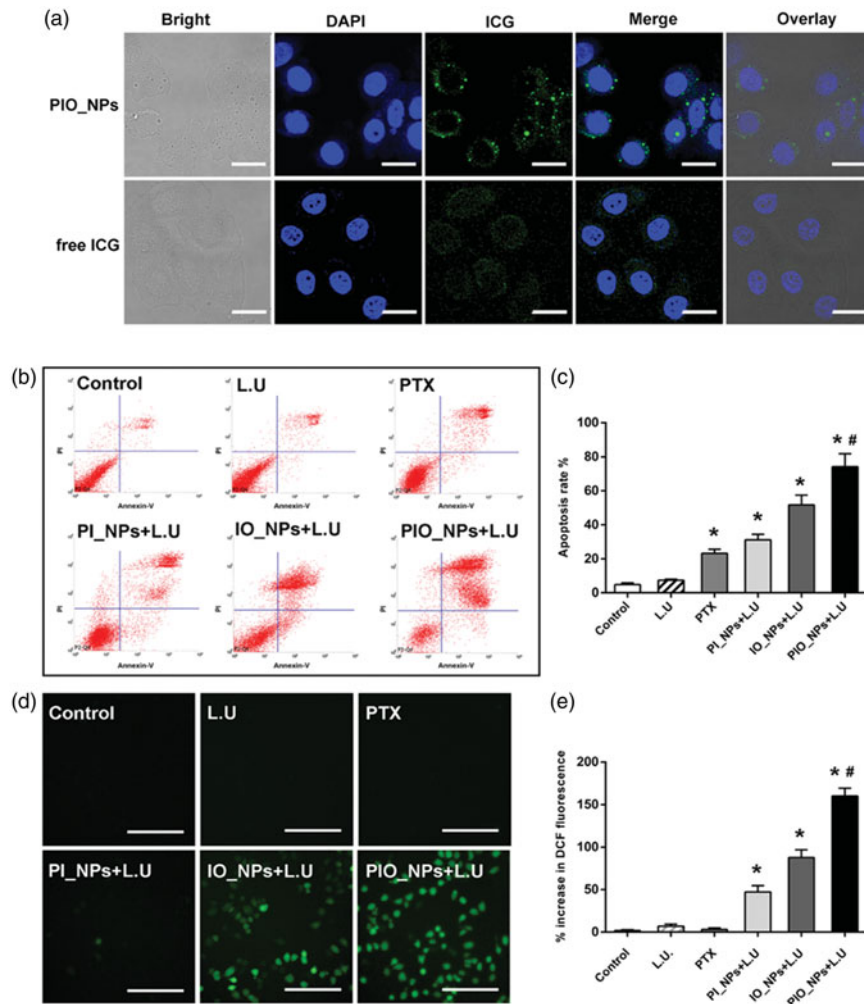


**Figure 2.** Cellular uptake of free ICG and PIO\_NPs by SKOV3 cells (a), scale bar is 20  $\mu$ m. Cell apoptosis in SKOV3 cells with different treatment (b). The percentage of apoptosis cells was determined by flow cytometry 24 h after treatment (c). Data were represented as mean  $\pm$  SD ( $n = 3$ ). Each treated group compared with control group, \* $p < .05$ ; PIO\_NPs + L.U group compared with other groups, # $p < .05$ . SKOV3 cell incubated with DCFH-DA staining for ROS detection by fluorescence microscopy images (d), scale bar is 50  $\mu$ m. Percentage increase of DCF fluorescence of distinct groups was (e). Each treated group compared with control group, \* $p < .05$ ; PIO\_NPs + L.U group compared with other groups, # $p < .05$ .

were more efficient for treatment. We also assessed the cytotoxicity of different treatment (Figure S4(b)). As a result, the cell viability of PIO\_NPs + L.U group was  $38.17 \pm 4.41\%$ , which was almost a half of PTX group. Cell viability of the PI\_NPs + L.U group and the IO\_NPs + L.U group was  $69.96 \pm 3.10\%$  and  $59.42 \pm 2.78\%$ , respectively, indicating that NPs without PTX loaded or oxygen carried exerted less effect on cell viability. In addition, it was shown that only exposure to L.U had no significant killing effect on the cells. The rate of apoptosis was quantified by flow cytometry (Figure 2(b,c)). The apoptotic trend was consistent with the cell inhibition rate in MTT assay for each group. To be specific, the apoptotic rate in the PIO\_NPs group reached  $74.09 \pm 7.64\%$ , while that the other groups did not exceed 50%. These results demonstrated that PIO\_NPs as a drug delivery system can combine the chemotherapeutic effects of PTX with the photo-sono dynamics of ICG.

Generation of ROS, as a primary factor to induce cell apoptosis in photo-sono dynamic treatment (Krafft, 2001; Riess, 2006; Polom et al., 2011; Porcu et al., 2016), was also detected (Figure 2(d,e)). After interacting with intracellular ROS, DCFH changed to DCF with green fluorescence. Cells

treated with PTX or only L.U hardly produced intracellular ROS. As confirmed by previous experiments, exposure of ICG-treated cells to NIR or ultrasound resulted in the production of ROS (Zheng et al., 2013). The NPs containing ICG (PI\_NPs, IO\_NPs, and PIO\_NPs) significantly increased intracellular DCF fluorescence under L.U. In PIO\_NPs + L.U group, the DCF fluorescence increased by  $160.04 \pm 9.20\%$ , higher than other NPs groups. This may be due to the oxygen it carried, which could be effectively triggered by NIR and ultrasound.

### 3.3. Imaging in vivo

In order to investigate the time of PIO\_NPs arriving and accumulating in tumor tissue, PA imaging was obtained at different times after PIO\_NPs injection (Figure S6). PA signal was enhanced at the tumor site after 2–12 h of injection, and it was the strongest at 6 h, indicating that the PIO\_NPs could accumulate in tumor tissue and enhance PA imaging. It also suggested that the L.U exposure should be performed after 6 h of PIO\_NPs injection. Afterward, we compared the PA signal between free ICG and PIO\_NPs groups (Figure 3). For

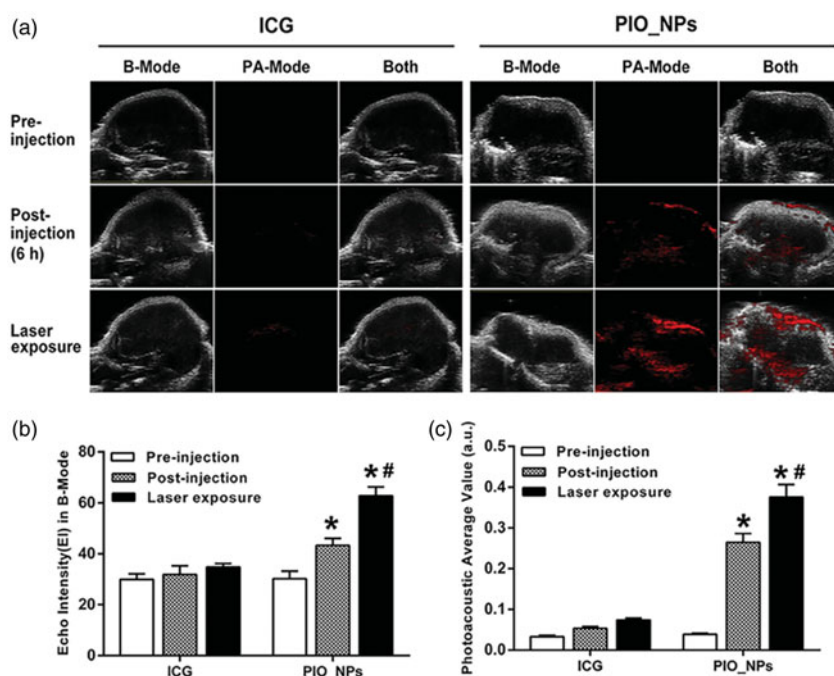


**Figure 3.** B-Mode and PA-Mode imaging of different groups before and after irradiation (a), echo intensity (b), and photoacoustic average value (c) were measured. Compared with pre-injection, echo intensity and PA value of PIO\_NPs group increased,  $*p < .001$ . And EI and PA value were increased significantly after irradiation,  $\#p < .05$ .

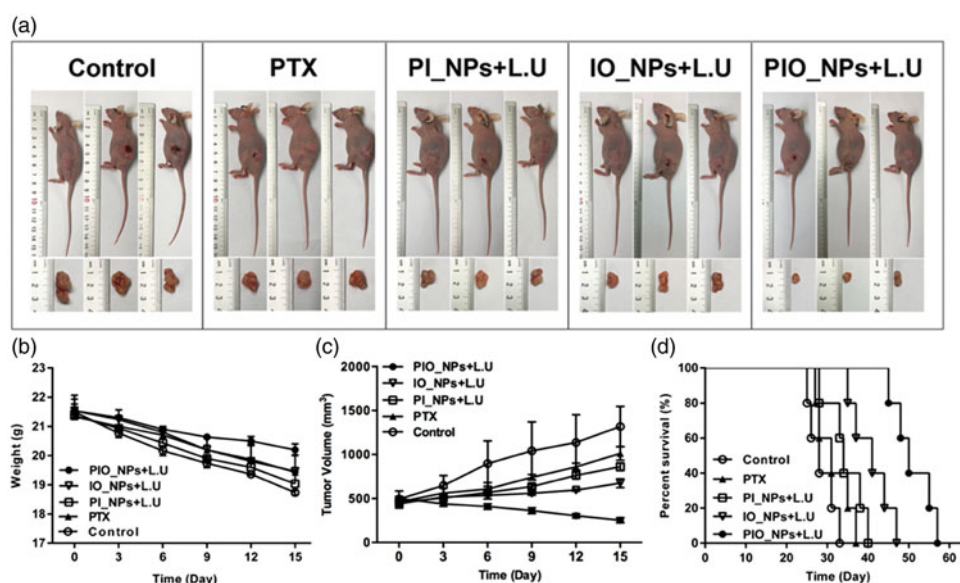


**Figure 4.** Growth inhibition of SKOV3 derived tumors in tumor xenograft models (a). During treatment, the body weight (b) and tumor volume (c) were recorded every 3 d. The tumors' volume in experimental groups was significantly smaller compared to that in the saline control group. The mice in PIO\_NPs+L.U group exhibited the slowest tumor growth rate. The survival curves of tumor-bearing mice treated in five groups (d). The median survival times of mice in PIO\_NPs+L.U group was longer compared with other groups ( $p < .05$ ).

PIO\_NPs group, photoacoustic average value (a.u.) was increased from  $0.26 \pm 0.02$  to  $0.37 \pm 0.03$  due to laser irradiation. It may be related to the vaporization of PFP and thermal expansion of tissues (Wilson et al., 2012). However, there was no obvious PA signal for free ICG group. Because the clearance process of ICG was rapid (Wang et al., 2013; Wang et al., 2018), the majority of ICG was cleared out of body after 6 h.

### 3.4. Therapeutic effect in vivo

During treatment, the tumors in the control group grew rapidly to  $\sim 1300 \text{ mm}^3$ . When treated with PTX alone, the tumor growth was slightly inhibited (Figure 4(a,c)). Although PTX is a type of chemotherapeutic agent for ovarian cancer, it requires high dosage to reach anticancer effect. In our study, the amount of single PTX did not achieve a satisfying anticancer effect. In addition, the hypoxic environment in solid tumor negatively affected the effectiveness of chemotherapy (McEwan et al., 2015). For PI\_NPs+L.U group, there was no

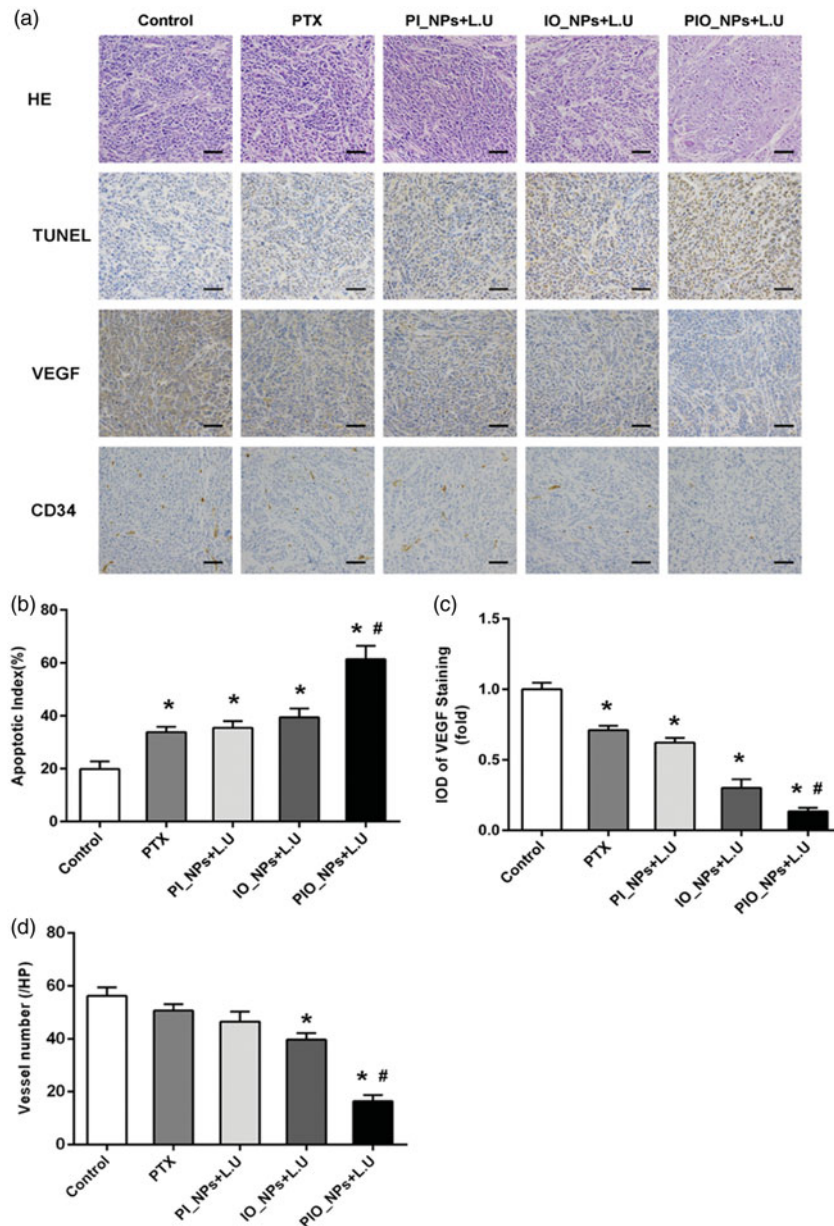


**Figure 5.** H&E staining, TUNEL assay, VEGF, and CD 34 immunohistochemical staining of tumor sections obtained 24 h after the last treatment from each group (a) scale bar is 50  $\mu$ m. For TUNEL assay, cancer cell that was brown in nuclei were counted as the apoptotic cells. The apoptotic index (AI) in each group (b). The slide integral optical density (IOD) of VEGF protein in each group (c). CD34 immunohistochemical staining, the number of microvessels (brown) were counted. Quantitative analysis of microvessel density (MVD) in each group (d). Compared with control group, \* $p < .005$ ; Compared with PIO\_NPs + L.U group, # $p < .05$ .

significant difference in tumor volume compared with the PTX group. Without PFCs core, the stability of NPs may decrease and subsequently lead to a premature release of the encapsulated PTX (Rapoport, 2012). Tumor volume in IO\_NPs + L.U group was not obviously increased. This may be due to the fact that IO\_NPs can induce PSDT. Notably, the PIO\_NPs + L.U group showed the optimal therapeutic effect with the tumor volume decreasing to about 250 mm<sup>3</sup>. These results indicated that PIO\_NPs harbored the ability to combine chemotherapy and PSDT. Moreover, the oxygen released from PIO\_NPs reduced hypoxia in tumor tissue (Liu et al., 2015) and improved the anti-tumor effects. During treatment, the average body weight (Figure 4(b)) of PIO\_NPs + L.U group was decreased by nearly 1 g, but it was decreased by about 4 g in control group. After treatment, all

remaining tumor-bearing mice were observed (Figure 4(d)). The corresponding median survival times in control, PTX, PI\_NPs + L.U, IO\_NPs + L.U and PIO\_NPs + L.U group were 28, 31, 34, 41, and 50 d. Survival time of mice in PIO\_NPs + L.U group was longer compared with other groups ( $p < .05$ ). All of these results demonstrated that the PIO\_NPs combined L.U enhanced the anti-tumor efficiency.

Furthermore, the H&E and immunohistochemistry (IHC) staining microscopic images of tumor sections were shown in Figure 5. In H&E staining images, there was obvious necrosis in PIO\_NPs + L.U group, showing nuclear pyknosis, karyorrhexis, and karyolysis. However, there was no apparent necrosis in control or PTX group. In addition, tumor cell apoptosis after treatment was detected by TUNEL assay. Nuclei of apoptosis in tumor cells appeared as brown. For PIO\_NPs + L.U



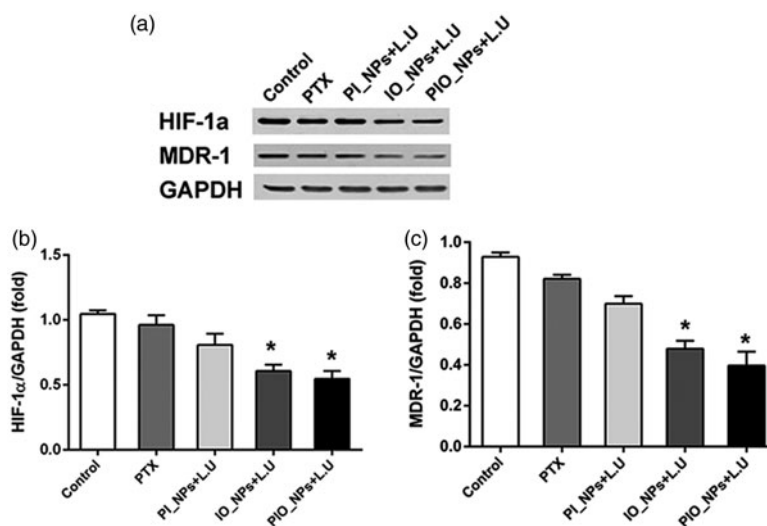


**Figure 6.** Expression of HIF-1 $\alpha$  and MDR-1 in tumor tissue was detected by western blot analysis 24 h after treatment. Quantification of band intensity of HIF-1 $\alpha$  expression relative to GAPDH was shown in columns (b). The intensity in control group to PIO\_NPs + L.U group were  $1.04 \pm 0.03$ ,  $0.96 \pm 0.07$ ,  $0.81 \pm 0.09$ ,  $0.60 \pm 0.05$ ,  $0.65 \pm 0.2$ , and  $0.54 \pm 0.06$ , respectively. Compared with control group,  $*p < .005$ . Quantification of band intensity of MDR-1 expression relative to GAPDH was shown in columns (c). The intensity in control group to PIO\_NPs + L.U group were  $0.92 \pm 0.02$ ,  $0.82 \pm 0.01$ ,  $0.70 \pm 0.03$ ,  $0.48 \pm 0.04$ , and  $0.40 \pm 0.07$ , respectively.

group, the strongest positive staining was displayed among all groups. Other groups displayed weak or moderate positive staining, respectively. Quantitative analysis of apoptosis indexes (AI) also proved the consistent conclusion. According to Figure 5(b), the apoptosis indexes (AI) for treatment group PBS, PTX, PI\_NPs + L.U and IO\_NPs + L.U are  $19.83 \pm 2.89$ ,  $33.73 \pm 2.02$ ,  $35.41 \pm 2.54$ , and  $39.43 \pm 3.29\%$ , respectively. Whereas this for PIO\_NPs + L.U was  $61.36 \pm 5.08\%$ , which was significantly higher compared with other treatment groups ( $p < .05$ ). These results indicated that L.U mediated delivery of PIO\_NPs significantly increased the tumor apoptosis efficiency.

As a key regulator of pathological angiogenesis, vascular endothelial growth factor (VEGF) contributes to growth and aggression of ovarian cancer (Masoumi Moghaddam et al., 2012). In our study, the expression of VEGF was detected by IHC staining (Figure 5), in which the positive cellular cytoplasm stained brown. The result showed that the expression of VEGF was the lowest in the PIO\_NPs + L.U group. Then, IOD of VEGF positive staining was quantitatively analyzed (Figure 5(c)). The IOD in groups PTX, PI\_NPs + L.U, and IO\_NPs + L.U were  $0.71 \pm 0.02$ ,  $0.62 \pm 0.01$ , and  $0.30 \pm 0.02$  fold of the control group, respectively. There was a statistically significant difference between each treatment group and the control group ( $p < .05$ ). Compared with PTX group, the VEGF expression was significantly inhibited in IO\_NPs + L.U or PIO\_NPs + L.U group, indicating that oxygen may be a relevant factor to reduce VEGF expression. The IOD of VEGF in PIO\_NPs + L.U group was  $0.13 \pm 0.01$  fold of the control group, which was the lowest among all groups. The low expression of VEGF demonstrated that angiogenesis in tumor can be effectively inhibited by the PIO\_NPs combined L.U treatment. We also detected the expression of CD34 to determine the MVD in tumor tissue (Figure 5(d)). The CD34-MVD of the control, PTX, PI\_NPs + L.U, and IO\_NPs + L.U groups were  $56.20 \pm 3.27$ ,  $50.67 \pm 2.42$ ,  $46.50 \pm 3.78$ , and  $39.67 \pm 2.42$ , respectively. For PIO\_NPs + L.U group, CD34-MVD was  $16.33 \pm 2.34$ , which was significantly lower than other groups

( $p < .05$ ). These results suggested that the PIO\_NPs combined with L.U could suppress the formation of new vessels in tumor and further inhibit the growth of tumor.

The expression of HIF-1 $\alpha$  and MDR-1 were detected by Western blot analysis (Figure 6). Compared with control group, the expression of HIF-1 $\alpha$  and MDR-1 was significantly decreased in the IO\_NPs + L.U group and the PIO\_NPs + L.U group. However, there was no significant difference in other groups. These results proved that oxygen-carrying nanoparticles can improve hypoxia and reduce chemoresistance in tumor tissues (Liu et al., 2015; McEwan, et al., 2015; McEwan et al., 2016).

#### 4. Conclusions

In summary, we constructed a type of phase-changeable nanoparticle that can carry oxygen and load ICG and PTX for ovarian cancer imaging and therapy. This nanoparticle preserved the optical properties of ICG and the chemotherapeutic effect of PTX, which also applied the phase-shift and carrying oxygen ability of PFP. And the PIO\_NPs realized controlled release of PTX and generation of ROS by near-infrared laser and low-intensity ultrasound exposure. Based on the encapsulation of ICG and PFP, the PIO\_NPs enhanced ultrasound and photoacoustic imaging. In addition, the accumulation of PIO\_NPs in the tumor can be observed by PA imaging. These results suggested that the PIO\_NPs might be a potential dual-mode imaging contrast agent, which can be used to monitor and guide treatment. The PIO\_NPs combined with L.U exposure demonstrated significant anti-tumor efficacy against SKOV3 cell line and tumor. The anti-tumor mechanisms are considered in the following three aspects: (1) L.U-triggered PTX release; (2) ICG-based PSDT, with ROS producing; (3) oxygen transport to tumor site to enhance therapeutic effect and reduce hypoxia. Therefore, the PIO\_NPs could be a promising drug delivery nanoplatform and imaging contrast agent, which might be used to realize integration of diagnosis and treatment for ovarian cancer.

## Acknowledgments

We are grateful to Dr. Ronald X. Xu (Department of Biomedical Engineering, The Ohio State University, Columbus, OH, USA) for technical advice, to Dr. Pan Li and Lan Hao (Institute of Ultrasound Imaging, Second Hospital of Chongqing Medical University, and Chongqing, China) for technical advice on appraisal of NIR and low-intensity ultrasound, to Dr. Tinghe Yu (Director of Key Medical laboratory of Obstetrics and Gynecology, The Second Affiliated Hospital, Chongqing Medical University, Chongqing, China) for the generous support of the experimental facilities.

## Disclosure statement

No potential conflict of interest was reported by the authors.

## Funding

This study was funded by National Natural Science Foundation of China [81572558, 81630047, and 31630026] and Health and Family Planning Commission Foundation of Chongqing [2015ZDXM010].

## ORCID

Shuning Chen  <http://orcid.org/0000-0002-3824-4815>

## References

- Abou-ElNaga A, Mutawa G, El-Sherbiny IM, et al. (2017). Novel nano-therapeutic approach actively targets human ovarian cancer stem cells after xenograft into nude mice. *Int J Mol Sci* 18:813.
- Chen J, Liu C, Zeng G, et al. (2016). Indocyanine green loaded reduced graphene oxide for in vivo photoacoustic/fluorescence dual-modality tumor imaging. *Nanoscale Res Lett* 11:85.
- Cho EC, Glaus C, Chen J, et al. (2010). Inorganic nanoparticle-based contrast agents for molecular imaging. *Trends Mol Med* 16:561–73.
- Cortez AJ, Tudrej P, Kujawa KA, et al. (2018). Advances in ovarian cancer therapy. *Cancer Chemother Pharmacol* 81:17–38.
- Deng L, Cai X, Sheng D, et al. (2017). A laser-activated biocompatible theranostic nanoagent for targeted multimodal imaging and photothermal therapy. *Theranostics* 7:4410–23.
- Di Meo S, Reed TT, Venditti P, et al. (2016). Role of ROS and RNS sources in physiological and pathological conditions. *Oxid Med Cell Longev* 2016:1245049.
- Gao C, Deng ZJ, Peng D, et al. (2016). Near-infrared dye-loaded magnetic nanoparticles as photoacoustic contrast agent for enhanced tumor imaging. *Cancer Biol Med* 13:349–59.
- Hannah A, Luke G, Wilson K, et al. (2014). Indocyanine green-loaded photoacoustic nanodroplets: dual contrast nanoconstructs for enhanced photoacoustic and ultrasound imaging. *ACS Nano* 8:250–9.
- Heo MB, Kim SY, Yun WS, Lim YT. (2015). Sequential delivery of an anticancer drug and combined immunomodulatory nanoparticles for efficient chemoimmunotherapy. *Int J Nanomedicine* 10:5981–92.
- Huang F, You M, Chen T, et al. (2014). Self-assembled hybrid nanoparticles for targeted co-delivery of two drugs into cancer cells. *Chem Commun* 50:3103–5.
- Kampan NC, Madondo MT, McNally OM, et al. (2015). Paclitaxel and its evolving role in the management of ovarian cancer. *Biomed Res Int* 2015:413076.
- Kim H, Kim Y, Kim IH, et al. (2013). ROS-responsive activatable photosensitizing agent for imaging and photodynamic therapy of activated macrophages. *Theranostics* 4:1–11.
- Krafft MP. (2001). Fluorocarbons and fluorinated amphiphiles in drug delivery and biomedical research. *Adv Drug Deliv Rev* 47:209–28.
- Lemaster JE, Jokerst JV. (2017). What is new in nanoparticle-based photoacoustic imaging? *Wires Nanomed Nanobiotechnol* 9:e1404.
- Li JH, Chen ZQ, Huang Z, et al. (2013). In vitro study of low intensity ultrasound combined with different doses of PDT: effects on C6 glioma cells. *Oncol Lett* 5:702–6.
- Lin S, Shah A, Hernández-Gil J, et al. (2017). Optically and acoustically triggerable sub-micron phase-change contrast agents for enhanced photoacoustic and ultrasound imaging. *Photoacoustics* 6:26–36.
- Liu L, Chang S, Sun J, et al. (2015). Ultrasound-mediated destruction of paclitaxel and oxygen loaded lipid microbubbles for combination therapy in ovarian cancer xenografts. *Cancer Lett* 361:147–54.
- Liu Y, Nie L, Chen X, et al. (2016b). Photoacoustic molecular imaging: from multiscale biomedical applications towards early-stage theranostics. *Trends Biotechnol* 34:420–33.
- Liu Y, Wang P, Liu Q, et al. (2016a). Sinoporphyrin sodium triggered sono-photodynamic effects on breast cancer both in vitro and in vivo. *Ultrason Sonochem* 31:437.
- Ma R, Wu Q, Si T, et al. (2017). Oxygen and indocyanine green loaded microparticles for dual-mode imaging and sonodynamic treatment of cancer cells. *Ultrason Sonochem* 39:197–207.
- Masoumi Moghaddam S, Amini A, Morris DL, et al. (2012). Significance of vascular endothelial growth factor in growth and peritoneal dissemination of ovarian cancer. *Cancer Metastasis Rev* 31:143–62.
- McEwan C, Fowley C, Nomikou N, et al. (2014). Polymeric microbubbles as delivery vehicles for sensitizers in sonodynamic therapy. *Langmuir* 30:14926–30.
- McEwan C, Kamila S, Owen J, et al. (2016). Combined sonodynamic and antimetabolite therapy for the improved treatment of pancreatic cancer using oxygen loaded microbubbles as a delivery vehicle. *Biomaterials* 80:20–32.
- McEwan C, Owen J, Stride E, et al. (2015). Oxygen carrying microbubbles for enhanced sonodynamic therapy of hypoxic tumours. *J Control Release* 203:51–6.
- Nomikou N, Sterrett C, Arthur C, et al. (2012). The effects of ultrasound and light on indocyanine-green-treated tumour cells and tissues. *ChemMedChem* 7:1465–71.
- Pakulska MM, Elliott Donaghue I, Obermeyer JM, et al. (2016). Encapsulation-free controlled release: electrostatic adsorption eliminates the need for protein encapsulation in PLGA nanoparticles. *Sci Adv* 2:e1600519.
- Polom K, Murawa D, Rho YS, et al. (2011). Current trends and emerging future of indocyanine green usage in surgery and oncology: a literature review. *Cancer* 117:4812–22.
- Porcu EP, Salis A, Gavini E, et al. (2016). Indocyanine green delivery systems for tumour detection and treatments. *Biotechnol Adv* 34:768–89.
- Raisch DW, Campbell W, Garg V, et al. (2011). Description of anaphylactic reactions to paclitaxel and docetaxel reported to the FDA, with a focus on the role of premedication. *Expert Opin Drug Saf* 10:521–8.
- Rapoport N. (2012). Phase-shift, stimuli-responsive perfluorocarbon nanodroplets for drug delivery to cancer. *Wiley Interdiscip Rev Nanomed Nanobiotechnol* 4:492–510.
- Riess JG. (2006). Perfluorocarbon-based oxygen delivery. *Artif Cells Blood Substit Immobil Biotechnol* 34:567–80.
- Siegel RL, Miller KD, Jemal A, et al. (2017). Cancer statistics, 2017. *CA Cancer J Clin* 67:7–30.
- Su S, Tian Y, Li Y, et al. (2015). “Triple-punch” strategy for triple negative breast cancer therapy with minimized drug dosage and improved antitumor efficacy. *ACS Nano* 9:1367–78.
- Sun Y, Wang Y, Niu C, et al. (2014). Laser-activatable PLGA microparticles for image-guided cancer therapy in vivo. *Adv Funct Mater* 24:7674–80.
- Tang Q, Cui J, Tian Z, et al. (2017). Oxygen and indocyanine green loaded phase-transition nanoparticle-mediated photo-sonodynamic cytotoxic effects on rheumatoid arthritis fibroblast-like synoviocytes. *Int J Nanomedicine* 12:381–93.
- Tew WP, Muss HB, Kimmick GG, et al. (2014). Breast and ovarian cancer in the older woman. *J Clin Oncol* 32:2553–61.
- Tomankova K, Kolarova H, Kolar P, et al. (2009). Study of cytotoxic effect of photodynamically and sonodynamically activated sensitizers in vitro. *Toxicol In Vitro* 23:1465–71.
- Torre LA, Bray F, Siegel RL, et al. (2015). Global cancer statistics, 2012. *CA Cancer J Clin* 65:87–108.

- Tserkovsky DA, Alexandrova EN, Chalau VN, Istomin YP. (2012). Effects of combined sonodynamic and photodynamic therapies with photolon on a glioma C6 tumor model. *Exp Oncol* 34:332–5.
- Valluru KS, Wilson KE, Willmann JK, et al. (2016). Photoacoustic imaging in oncology: translational preclinical and early clinical experience. *Radiology* 280:332–49.
- Wang H, Li X, Tse BWC, et al. (2018). Indocyanine green-incorporating nanoparticles for cancer theranostics. *Theranostics* 8:1227–42.
- Wang P, Li C, Wang X, et al. (2015). Anti-metastatic and pro-apoptotic effects elicited by combination photodynamic therapy with sonodynamic therapy on breast cancer both in vitro and in vivo. *Ultrason Sonochem* 23:116–27.
- Wang X, Zhang W, Xu Z, et al. (2009). Sonodynamic and photodynamic therapy in advanced breast carcinoma: a report of 3 cases. *Integr Cancer Ther* 8:283–7.
- Wang YW, Fu YY, Peng Q, et al. (2013). Dye-enhanced graphene oxide for photothermal therapy and photoacoustic imaging. *J Mater Chem B* 1:5762–7.
- Wilson K, Homan K, Emelianov S, et al. (2012). Biomedical photoacoustics beyond thermal expansion using triggered nanodroplet vaporization for contrast-enhanced imaging. *Nat Commun* 3:618.
- Zhang N, Cai X, Gao W, et al. (2016). A multifunctional theranostic nanoagent for dual-mode image-guided HIFU/chemo- synergistic cancer therapy. *Theranostics* 6:404–17.
- Zheng M, Yue C, Ma Y, et al. (2013). Single-step assembly of DOX/ICG loaded lipid-polymer nanoparticles for highly effective chemo-photothermal combination therapy. *ACS Nano* 7:2056–67.
- Zheng X, Xing D, Zhou F, et al. (2011). Indocyanine green-containing nanostructure as near infrared dual-functional targeting probes for optical imaging and photothermal therapy. *Mol Pharm* 8:447–56.